Acta Cryst E CRYSTALLOGRAPHIC COMMUNICATIONS

ISSN 2056-9890

3,3-Bis(2-hydroxyethyl)-1-(4-nitrobenzoyl)thiourea: crystal structure, Hirshfeld surface analysis and computational study

Sang Loon Tan,[a] Mukesh M. Jotani[b] and Edward R. T. Tiekink[a]*

[a]Research Centre for Crystalline Materials, School of Science and Technology, Sunway University, 47500 Bandar Sunway, Selangor Darul Ehsan, Malaysia, and [b]Department of Physics, Bhavan's Sheth R. A. College of Science, Ahmedabad, Gujarat 380001, India. *Correspondence e-mail: edwardt@sunway.edu.my

Received 27 December 2019
Accepted 29 December 2019

Edited by W. T. A. Harrison, University of Aberdeen, Scotland

Keywords: crystal structure; thiourea; nitro group; hydrogen bonding; Hirshfeld surface analysis; computational chemistry.

CCDC reference: 1919879

Supporting information: this article has supporting information at journals.iucr.org/e

In the title compound, $C_{12}H_{15}N_3O_5S$, a trisubstituted thiourea derivative, the central CN_2S chromophore is almost planar (r.m.s. deviation = 0.018 Å) and the pendant hydroxyethyl groups lie to either side of this plane. While to a first approximation the thione-S and carbonyl-O atoms lie to the same side of the molecule, the S—C—N—C torsion angle of −47.8 (2)° indicates a considerable twist. As one of the hydroxyethyl groups is orientated towards the thioamide residue, an intramolecular N—H···O hydrogen bond is formed which leads to an *S*(7) loop. A further twist in the molecule is indicated by the dihedral angle of 65.87 (7)° between the planes through the CN_2S chromophore and the 4-nitrobenzene ring. There is a close match between the experimental and gas-phase, geometry-optimized (DFT) molecular structures. In the crystal, O—H···O and O—H···S hydrogen bonds give rise to supramolecular layers propagating in the *ab* plane. The connections between layers to consolidate the three-dimensional architecture are of the type C—H···O, C—H···S and nitro-O···π. The nature of the supramolecular association has been further analysed by a study of the calculated Hirshfeld surfaces, non-covalent interaction plots and computational chemistry, all of which point to the significant influence and energy of stabilization provided by the conventional hydrogen bonds.

1. Chemical context

In addition to accepting C—H···O interactions, nitro groups are known to form nitro-N—O···π(aryl) interactions (Huang *et al.*, 2008) as well as participate as donors and acceptors in π-hole interactions (Bauzá *et al.*, 2014). Hence, when the title nitro-containing compound, (I), became available, a crystallographic analysis was undertaken. Compound (I) is an example of a tri-substituted thiourea molecule, $H_2NC(=S)NH_2$, whereby three of the four hydrogen atoms have been substituted to yield 4-$NO_2C_6H_4C(=O)N(H)C(=S)N(CH_2CH_2OH)_2$. Such *N*,*N*′-di(alkyl/aryl)-*N*′-benzoylthiourea derivatives have a carbonyl group connected to the thiourea framework and offer opportunities for rich coordination chemistry as these molecules feature both hard (oxygen) and soft (sulfur) donor atoms along with nitrogen donors and indeed, a variety of coordination modes have been observed. The neutral molecule has been observed to coordinate in a monodentate-*S* mode (Gunasekaran, Ng *et al.*, 2012; Saeed *et al.*, 2014). In its deprotonated form, *O*-,*S*-chelation is often observed (Saeed *et al.*, 2014). There are a variety of motivations for investigating metal complexes of benzoylthiourea derivatives such as for catalytic applications and for anion recognition (Zhang & Schreiner, 2009; Guna-

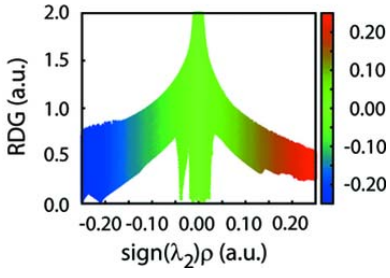

sekaran, Jerome *et al.*, 2012; Nishikawa, 2018). Over and above these considerations, there are continuing investigations into their biological potential, such as anti-microbial (Gemili *et al.*, 2017; Binzet *et al.*, 2018; Saeed *et al.*, 2018), anti-cancer (Peng *et al.*, 2016; Barolli *et al.*, 2017; Jeyalakshmi *et al.*, 2019) and anti-mycobacterium tuberculosis (Plutín *et al.*, 2016) agents. In a continuation of our on-going work on these molecules and their metal complexes (Selvakumaran, Ng *et al.*, 2011; Selvakumaran, Karvembu *et al.*, 2011; Gunasekaran *et al.*, 2017; Tan, Azizan *et al.*, 2019), we now describe the synthesis, spectroscopic characterization and X-ray crystallographic investigation of (I). Further, an analysis of the calculated Hirshfeld surfaces, non-covalent interaction plots as well as a computational chemistry study for (I) are described.

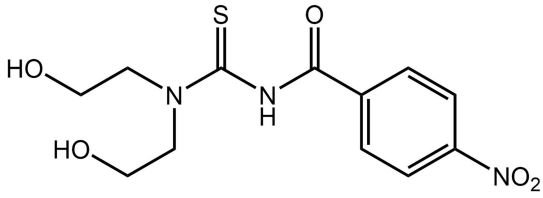

2. Structural commentary

Selected geometrical data for (I), Fig. 1, are given in Table 1. The key feature of the structure is that it is a tri-substituted thiourea molecule with one of the nitrogen atoms having a benzoyl residue and the other bearing two hydroxyethyl groups. An approximate *syn* relationship is established between the thione-S and carbonyl-O atoms. Even though they lie to the same side of the molecule, the S1—C1—N2—C6 torsion angle of −47.8 (2)° is consistent with a significant twist in the molecule about the C1—N2 bond; the O3—C6—N2—C1 torsion angle is −3.6 (2)°.

The hydroxyethyl groups lie to either side of the CN_2S plane (r.m.s. deviation = 0.017 Å). Crucially, the O1-hydroxyethyl group is folded towards the thioamide residue, which allows for the formation of an intramolecular N2—H···O1 hydrogen bond and an *S*(7) loop, Table 2. That the molecule is highly twisted is evidenced by the dihedral angle of 65.87 (7)° between the CN_2S atoms and the terminal C7–C12 aryl ring. From Table 1, it is apparent that the C1—N1 bond length is considerably shorter than C1—N2, indicating delocalization of π-electron density over the S1—C1—N1 atoms. However, the large twist for the C1—N2 bond mentioned above does not allow significant delocalization to extend to atoms C1, N1 and C6. The expected trends relating to the nature of the bonds about the quaternary-C1 atom are seen in the bond angles about that atom. Thus, the angles subtended by the formally doubly bonded S1 atom are appreciably wider. Finally, the nitro group is effectively co-planar with the aryl ring to which it is attached, as seen in the O4—N3—C10—C9 torsion angle of 5.2 (2)°.

Table 1
Selected geometric parameters (Å, °) for (I) determined experimentally (X-ray) and from theory (DFT).

Parameter	X-ray	Theory
C1═S1	1.6777 (16)	1.668
C1—N1	1.334 (2)	1.366
C1—N2	1.4038 (19)	1.410
C6—O3	1.2156 (18)	1.219
C6—N2	1.3771 (19)	1.388
S1—C1—N1	123.83 (12)	124.7
S1—C1—N2	121.89 (11)	121.8
N1—C1—N2	114.23 (13)	113.4
O3—C6—N2	123.57 (14)	124.3
O3—C6—C7	121.17 (13)	121.1
N2—C6—C7	115.20 (13)	114.5
S1—C1—N2—C6	−47.8 (2)	−44.6
S1—C1—N1—C2	173.80 (11)	167.8
S1—C1—N1—C4	−8.0 (2)	−7.2
O3—C6—N2—C1	−3.6 (2)	−16.5
O3—C6—C7—C8	163.29 (15)	152.7
N1—C2—C3—O1	−62.76 (17)	−69.3
N1—C4—C5—O2	57.76 (17)	68.4

3. Gas-phase theoretical structure

With the aid of a long-range corrected wB97XD density functional with Grimme's D2 dispersion model (Chai & Head-Gordon, 2008) and coupled with Pople's 6-311+G(*d*,*p*) basis

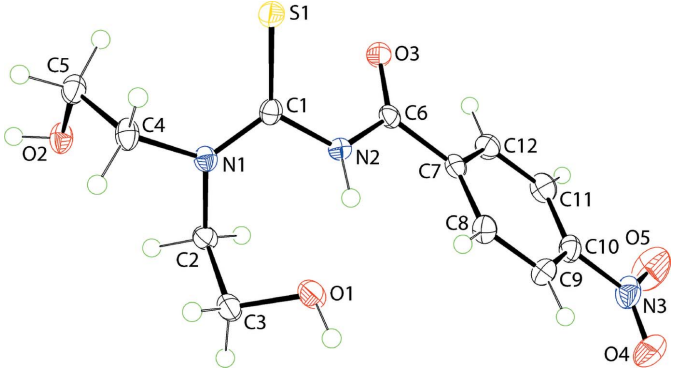

Figure 1
The molecular structure of (I) showing the atom-labelling scheme and displacement ellipsoids at the 70% probability level.

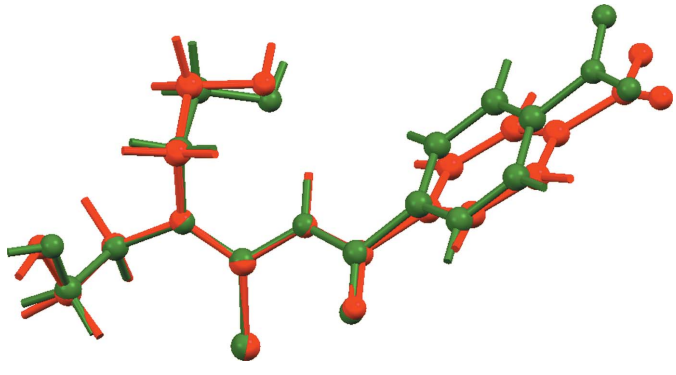

Figure 2
Overlay diagram for the experimental (green image) and geometry-optimized (red) molecules of (I). The molecules have been overlapped so the S═C—N—C═O fragments are coincident.

set (Petersson *et al.*, 1988), as implemented in *Gaussian16* (Frisch *et al.*, 2016), the gas-phase geometry-optimized structure of (I) was calculated. As confirmed through a frequency analysis with zero imaginary frequency, the local minimum structure in the gas-phase was located in this study. The experimental and theoretical structures are superimposed (Macrae *et al.*, 2006) in Fig. 2. The analysis shows that there are only minor differences between the molecules with the r.m.s. deviation between the conformations being only 0.015 Å. The derived interatomic data for the geometry-optimized structure are included in Table 1 from which it can be seen there is a close correlation between the experimental and calculated geometries.

It is evident that the only major differences between the experimental and geometry-optimized structures relate to some of the torsion angles. Thus, the most significant conformational difference is evidenced by a nearly 13° difference in the O3—C6—N2—C1 torsion angles, *i.e.* −3.6 (2)° (X-ray) *versus* −16.5° (calculation), indicating a greater deviation from the *anti*-disposition in the optimized structure. Also, the N1—C2—C3—O1 and N1—C4—C5—O2 torsion angles are close to symmetric in the optimized structure *cf.* the experimental structure. Similar trends were noted in analogous calculations performed on the 4-methyl analogue (Tan, Azizan *et al.*, 2019).

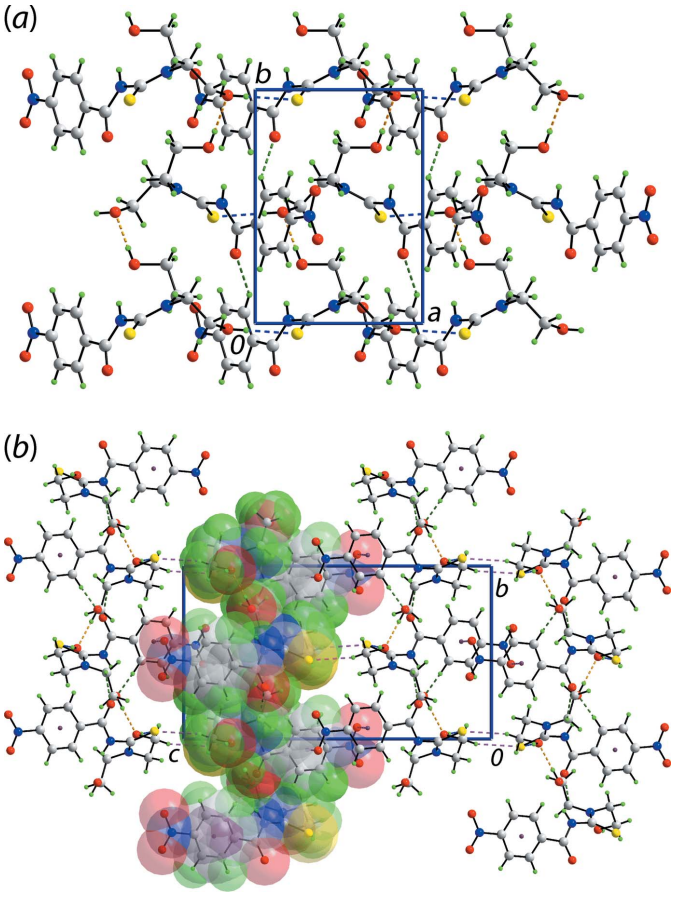

Figure 3
Views of the molecular packing in (I): (*a*) supramolecular layer in the *ab* plane sustained by hydroxy-O—H···O(hydroxy) and hydroxy-O—H···S(thione) hydrogen bonds and (*b*) view of the unit-cell contents in a projection down the *a* axis, highlighting the methylene-C—H···O(carbonyl), methylene-C—H···S(thione) and nitro-O···π(aryl) connections between layers; one layer is represented in space-filling mode. The O—H···O, O—H···S, C—H···O, C—H···S and N—O···π interactions are shown as orange, blue, green, pink and purple dashed lines, respectively.

Table 2
Hydrogen-bond geometry (Å, °).

*Cg*1 is the centroid of the (C7–C12) ring.

D—H···*A*	*D*—H	H···*A*	*D*···*A*	*D*—H···*A*
N2—H2*N*···O1	0.87 (1)	1.88 (1)	2.6749 (17)	151 (1)
O1—H1*O*···O2^{i}	0.84 (2)	1.87 (2)	2.7075 (17)	176 (2)
O2—H2*O*···S1^{ii}	0.84 (1)	2.33 (1)	3.1724 (12)	175 (2)
C2—H2*B*···O3^{i}	0.99	2.53	3.2305 (18)	127
C5—H5*A*···S1^{iii}	0.99	2.77	3.4915 (17)	130
C8—H8···O3^{iv}	0.95	2.36	3.2147 (19)	150
N3—O4···*Cg*1^{v}	1.22 (1)	3.63 (1)	3.6927 (16)	83 (1)

Symmetry codes: (i) $-x+1, y+\frac{1}{2}, -z+\frac{3}{2}$; (ii) $x-1, y, z$; (iii) $-x+1, -y+1, -z+1$; (iv) $-x+2, y+\frac{1}{2}, -z+\frac{3}{2}$; (v) $-x+2, -y+1, -z+2$.

4. Supramolecular features

In the crystal of (I), O1—H1*O*···O2 hydrogen bonds (Table 2) lead to a helical chain propagating along the *b*-axis direction, with adjacent molecules related by the 2_1 screw axis. The O2—H2*O*···S1 hydrogen bonding serves to cross-link translationally related chains along the *a* axis to form a supramolecular layer in the *ab* plane, Fig. 3(*a*). The layers are connected into a three-dimensional architecture by methylene-C—H···O(carbonyl), methylene-C—H···S(thione) and comparatively rare nitro-O···π(aryl) contacts, Fig. 3(*b*).

5. Hirshfeld surface analysis

Using *Crystal Explorer 17* (Turner *et al.*, 2017) and established procedures (Tan, Jotani *et al.*, 2019), the Hirshfeld surfaces and two-dimensional fingerprint plots (full and decomposed)

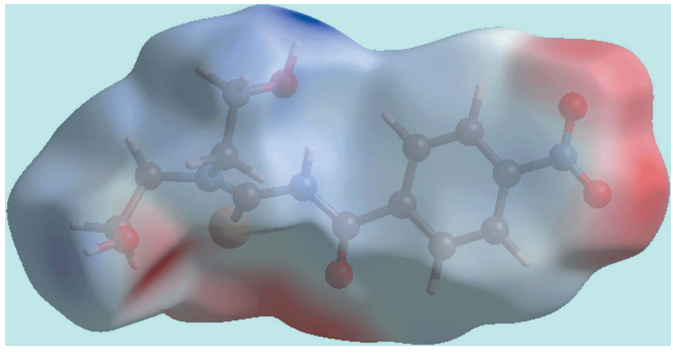

Figure 4
A view of the Hirshfeld surface mapped over the calculated electrostatic potential for (I). The red and blue regions represent negative and positive electrostatic potentials, respectively. The potentials were calculated using the STO-3G basis set at Hartree–Fock level of theory over a range of ±0.18 atomic units.

Table 3
A summary of short interatomic contacts (Å) in (I)[a].

Contact	Distance	Symmetry operation
H1*O*···H2*O*	2.23	$1-x, \frac{1}{2}+y, \frac{3}{2}-z$
C1···C3	3.368 (2)	$1-x, -\frac{1}{2}+y, \frac{3}{2}-z$
C1···H3*B*	2.71	$1-x, -\frac{1}{2}+y, \frac{3}{2}-z$
C3···O3	3.0819 (19)	$1-x, \frac{1}{2}+y, \frac{3}{2}-z$
C3···O5	3.168 (2)	$2-x, 1-y, 1-z$
H3*B*···O5	2.65	$2-x, 1-y, 1-z$
C5···H1*O*	2.61	$1-x, -\frac{1}{2}+y, \frac{3}{2}-z$
C6···O2	3.0924 (18)	$1+x, y, z$
C6···H2*O*	2.81	$1+x, y, z$

Note: (*a*) The interatomic distances are calculated in *Crystal Explorer 17* (Turner *et al.*, 2017) whereby the *X*—H bond lengths are adjusted to their neutron values.

for (I) were calculated. In the Hirshfeld surface mapped over electrostatic potential in Fig. 4, the donors and acceptors of the conventional O—H···O and O—H···S hydrogen bonds and C—H···O contacts appear as blue (positive potential) and red (negative potential) regions, respectively. The bright-red spots near the participating atoms in the Hirshfeld surface mapped over d_{norm} in Fig. 5 also give indications of these intermolecular interactions. Additional diminutive red spots near the methylene-H2*B* and H5*A*, thione-S1 and carbonyl-O3 atoms are indicative of weaker C—H···S and C—H···O

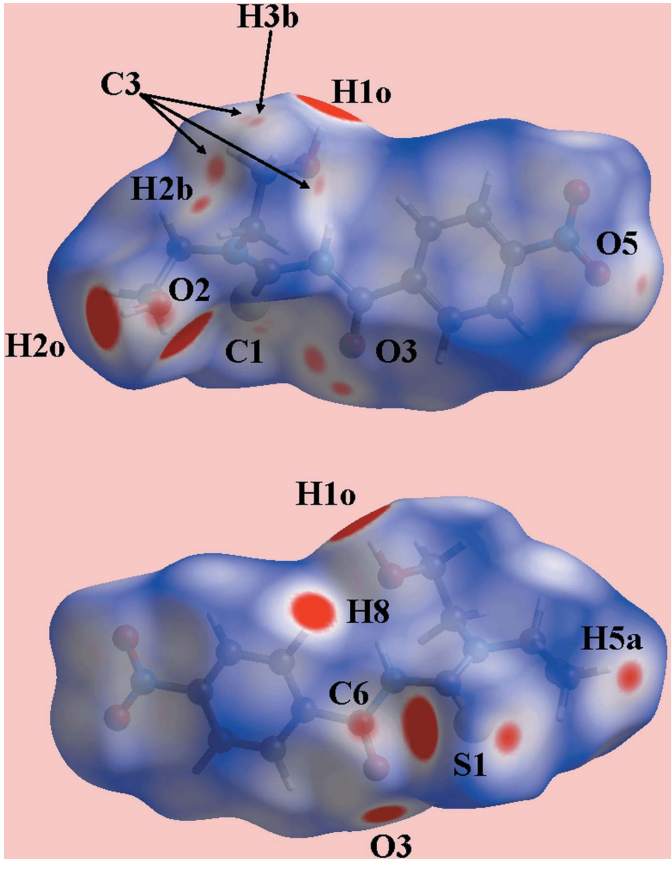

Figure 5
Two views of the Hirshfeld surface mapped over d_{norm} for (I) in the range −0.127 to +1.259 arbitrary units.

Table 4
Enrichment ratios for (I).

Parameter	Ratio
H···H	0.88
C···H	0.85
O···H	1.26
S···H	1.66
C···O	1.34

interactions, Table 2. Further, the presence of faint-red spots near the ethyl-C3 and nitro-O5 atoms on the surface indicate C—H···O contacts in the packing involving the nitro substituent. The other faint-red spots appearing in Fig. 5 indicate the presence of short interatomic contacts as summarized in Table 3. The influence of the nitro group is also seen in the nitro-O4···π(C7–C12) interaction, illustrated through yellow dotted lines in Fig. 6.

The enrichment ratio (ER) descriptor, which is derived from the analysis of the Hirshfeld surface (Jelsch *et al.*, 2014), was also employed to analyse the intermolecular contacts in the crystal of (I). The ER(*X*, *Y*) reflects the relative likelihood of the formation of *X*-to-*Y* interactions in a crystal, *i.e.* the ratio between the proportion of actual contacts in a crystal to the theoretical proportion of random contacts. Data for (I) are given in Table 4. The enrichment ratios greater than unity for the atom pairs (O, H) and, in particular, (S, H), are consistent with the relatively high likelihood for the formation of the O—H···O and O—H···S hydrogen bonds in the crystal of (I). It is also evident that the value greater than unity for (C, O) arises from the nitro-O···π(aryl) contacts.

The overall fingerprint plots for (I) and those delineated into H···H, O···H/H···O, C···H/H···C, S···H/H···S and C···O/O···C contacts are illustrated in Fig. 7(*a*)–(*f*), respectively, with a summary of the percentage contributions from

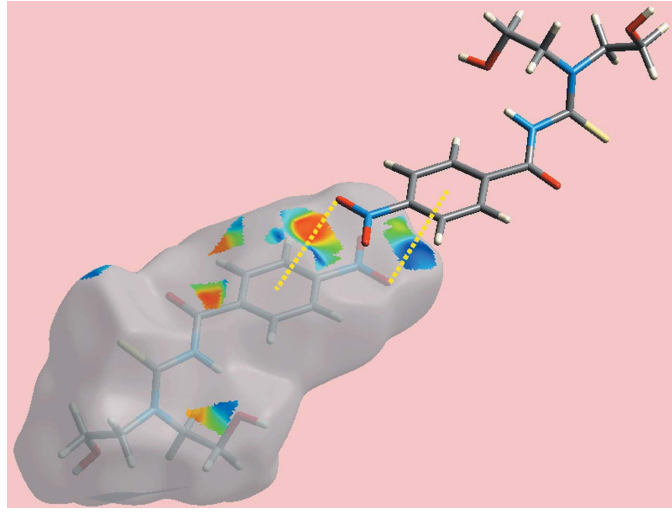

Figure 6
A view of the Hirshfeld surfaces mapped with the shape-index property for (I), highlighting the intermolecular N—O···π(aryl) interactions through yellow dotted lines.

Table 5
Percentage contributions of interatomic contacts to the Hirshfeld surface for (I).

Contact	Percentage contribution
H···H	31.8
O···H/H···O	30.7
C···H/H···C	10.3
S···H/H···S	13.9
C···O/O···C	5.8
N···H/H···N	1.9
O···O	1.6
C···N/N···C	1.5
C···C	1.3
N···O/O···N	0.9
N···N	0.3

the various contacts given in Table 5. The greatest contribution to the overall surface is from H···H contacts and this is closely followed by O···H/H···O contacts, as viewed by the pair of long spikes at $d_e + d_i$ ~1.8 Å in Fig. 7(*c*). The prominent features in Fig. 7(*d*) reflect the significant C···H/H···C contacts evident in the packing, Tables 2 and 3. The significant percentage contribution from S···H/H···S contacts reflects the presence of O—H···S hydrogen bonding and is apparent through the appearance of asymmetric spikes of different shapes at $d_e + d_i$ ~2.1 Å in the fingerprint plot of Fig. 7(*e*). The 5.8% contribution from C···O/O···C contacts and the aforementioned ER value of 1.66 clearly indicate the significance of the nitro-N—O···π interaction upon the packing; this interaction is reflected in the pair of short spikes $d_e + d_i$ ~3.0 Å, Fig. 7(*f*).

Table 6
Summary of interaction energies (kcal mol^{-1}) calculated for several directional contacts in (I).

Contact	E_{tot}
O1—H1*O*···O2	−14.04
O2—H2*O*···S1	−5.60
C8—H8···O3	−10.05

6. Computational chemistry

The energy calculations were performed using DFT-wB97XD/aug-cc-pVTZ (Woon & Dunning, 1993) to evaluate the strength of the intermolecular O—H···O, O—H···S and C—H···O interactions between the respective pairs of molecules. The BSSE corrected interaction energies (E^{BSSE}_{int}) are listed in Table 6. From these data, it is clear the O—H···O hydrogen bond has the greatest interaction energy, followed by C—H···O and O—H···S. These results reflect those reported recently for the 4-methyl analogue (Tan, Azizan *et al.*, 2019).

The non-covalent interaction plots generated by calculations performed with *NCIPLOT* (Johnson *et al.*, 2010) provide complementary results for the interaction energies. Thus, the pairs of molecules associated with each of the energies tabulated in Table 6 were subjected to calculation as this provides a useful visualization index corresponding to the strength of any non-covalent interactions through a red–blue–green colour scheme on the isosurface. Thus, a blue coloration is indicative of a strong attractive interaction, green indicates a weak interaction while red is indicative of a strong repulsive interaction (Contreras-García *et al.*, 2011). As seen from Fig. 8, the

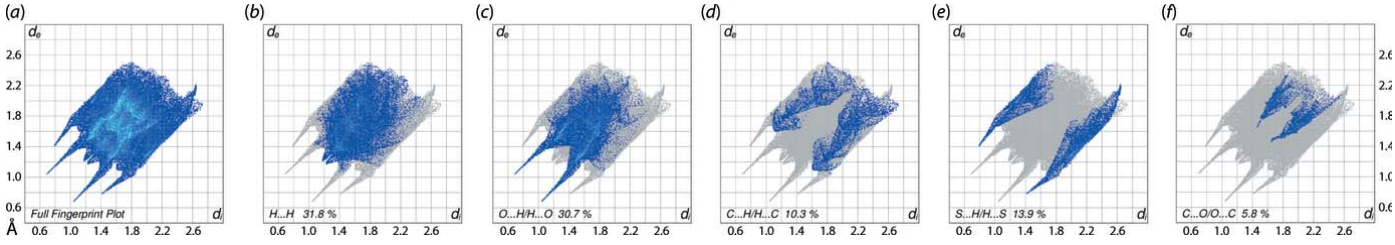

Figure 7
(*a*) A comparison of the full two-dimensional fingerprint plot for (I) and those delineated into (*b*) H···H, (*c*) O···H/H···O, (*d*) C···H/H···C, (*e*) S···H/H···S and (*f*) C···O/O···C contacts.

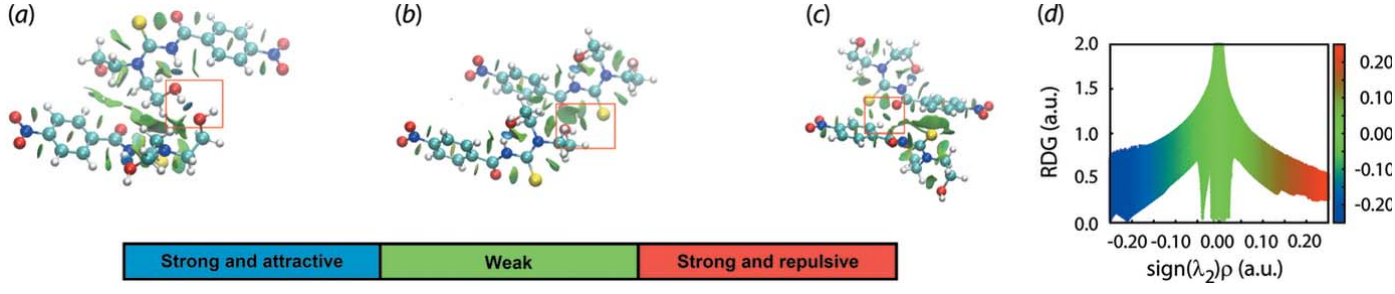

Figure 8
The non-covalent interaction (NCI) plots for the dimeric aggregates in (I) sustained by (*a*) O—H···O, (*b*) O—H···S and (*c*) C—H···O interactions (highlighted in boxes) and (*d*) plot of RDG versus sign(λ^2)ρ(r). The gradient cut-off is set at 0.4 and the colour scale is $-0.03 < \rho < 0.03$ atomic units.

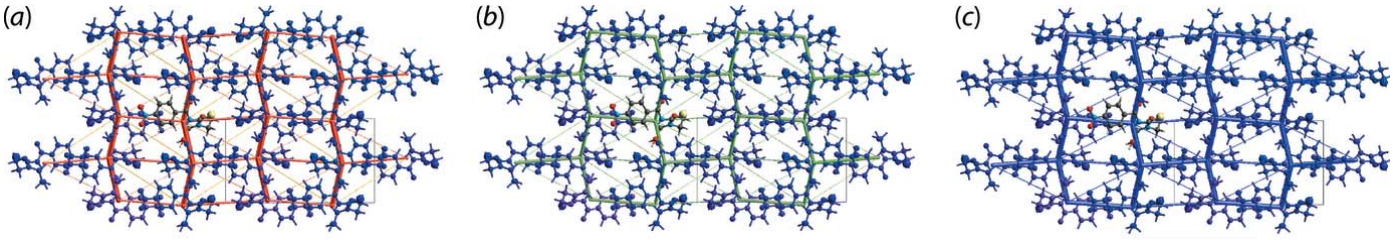

Figure 9
The energy framework diagrams for (I) showing (*a*) $E_{electrostatic}$ (red cylinders), (*b*) $E_{dispersion}$ (green cylinders) and (*c*) E_{total} (blue cylinders), viewed along the *a* axis. The frameworks were adjusted to the same scale factor of 50 with a cut-off value of 2.39 kcal/mol within 2 × 2 × 2 unit cells. The corresponding cylinder radii are proportional to the relative magnitude of the energies.

O—H···O interaction is clearly strong and attractive, while each of O—H···S and C—H···O are less so.

From the aforementioned, the molecular packing is clearly governed by directional hydrogen bonding between molecules. The simulated energy frameworks (Turner *et al.*, 2017) were calculated to compare the topology of the intermolecular interactions in the crystal of (I). An analysis of the resultant energy frameworks is shown in Fig. 9 and reveals the crystal of (I) is mainly stabilized by electrostatic and dispersive forces. The total electrostatic energy ($E_{electrostatic}$) of all pairwise interactions sums to −45.89 kcal/mol, while the total dispersion energy term ($E_{dispersion}$) computes to −51.51 kcal/mol.

7. Database survey

There are three literature precedents to (I), *i.e.* molecules of the general formula 4-*Y*C$_6$H$_4$C(=O)N(H)C(=S)N(CH$_2$CH$_2$OH)$_2$, namely *Y* = H, which has been reported twice (Koch *et al.*, 1995; Cornejo *et al.*, 2005), *Y* = F (Hennig *et al.*, 2009) and *Y* = Me (Tan, Azizan *et al.*, 2019). As seen in the overlay diagram of Fig. 10, whereby the central CN$_2$S residues are overlapped, there is a very close coincidence in the molecular structures. The differences in conformation are most conveniently expressed in terms of the dihedral angles formed between the central CN$_2$S chromophore and pendant aryl ring, *i.e.* 65.92 (12), 68.96 (12), 69.51 (8) and 72.15 (10)° for (I) and *Y* = H, F and Me, respectively.

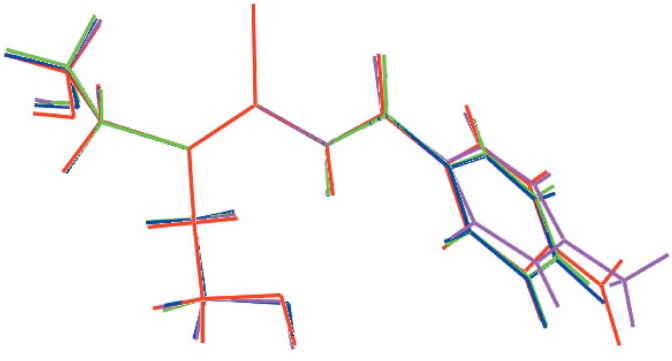

Figure 10
An overlay diagram of the four known structures of general formula 4-*Y*C$_6$H$_4$C(=O)N(H)C(=S)N(CH$_2$CH$_2$OH)$_2$: *Y* = NO$_2$ (I) red image, *Y* = H (green), *Y* = F (blue) and *Y* = Me (pink). The molecules are overlapped so the central CN$_2$S residues are coincident.

The molecular packing in the crystals is also very similar with the formation of the intramolecular thioamide-N—H···O(hydroxy) hydrogen bond as well as the intermolecular hydroxy-O—H···O(hydroxy) hydrogen and hydroxy-O—H···S(thione) hydrogen bonding, leading to a supramolecular layer in each case.

8. Synthesis and crystallization

Synthesis of (I): an excess of thionyl chloride (Merck) was mixed with 4-nitrobenzoic acid (Merck, 1 mmol) and the resulting solution was refluxed until a pale-yellow solution was obtained. The excess thionyl chloride was removed on a water bath, leaving only 4-nitrobenzoyl chloride, which is a yellow, viscous liquid. Ammonium thiocyanate (Fisher, 1 mmol) was added to an acetone (30 ml) solution of 4-nitrobenzoyl chloride (1 mmol). The solution turned yellow after stirring for 2 h. The white precipitate (ammonium chloride) was isolated upon filtration and to the yellow filtrate, bis(hydroxyethyl)amine (Acros, 1 mmol) was carefully added followed by stirring for 1 h. Upon the addition of dichloromethane (50 ml), a yellow precipitate was obtained, which was collected by filtration. Recrystallization was from its hot acetone solution yielding pale-yellow blocks of (I) after slow evaporation. Yield 69%. M.p. (Hanon MP-450 melting point apparatus): 411.5–413.7 K. IR (Bruker Vertex 70v FT–IR spectrophotometer, cm^{-1}): 3277 (*br*, νOH), 3170 (*br*, νNH), 3077 (*w*, νCH$_{aro}$), 2973–2882 (*w*, νCH), 1692 (*s*, νC=O), 1538 (*s*, νN=O$_{asym}$), 1524 (*s*, νC=C), 1343 (*s*, νN=O$_{sym}$), 1270 (*s*, νC—N), 1053 (*s*, νC=S), 734 (*s*, δCH). UV (Shimadzu UV 3600 Plus UV–vis spectrophotometer; ethanol:acetonitrile (1/1): λ$_{max}$ nm (log ε) 366.4 (4.16), 301.6 (4.88), 271.2 (5.00), 205.8 (5.14).

The pyrolytic process (Perkin Elmer STA 6000 Simultaneous Thermogravimetric Analyzer) for (I) showed the liberation of NO$_2$, equivalent a 15% weight loss, in the first stage in the range 194 and 222°C. This was followed by the liberation of a benzene molecule, corresponding to 29% weight loss, between 222 and 282°C, whereas the subsequent stages involve the pyrolysis of CO (282 to 360°C) and OH (360 to 496°C) corresponding to 15 and 11% weight loss, respectively. Gradual weight loss continued beyond 800°C.

Table 7
Experimental details.

Crystal data	
Chemical formula	$C_{12}H_{15}N_3O_5S$
M_r	313.33
Crystal system, space group	Monoclinic, $P2_1/c$
Temperature (K)	100
a, b, c (Å)	7.4203 (2), 10.3241 (3), 18.4191 (6)
β (°)	95.471 (2)
V (Å^3)	1404.62 (7)
Z	4
Radiation type	Mo $K\alpha$
μ (mm^{-1})	0.26
Crystal size (mm)	0.12 × 0.11 × 0.09
Data collection	
Diffractometer	Bruker *SMART APEX* diffractometer
Absorption correction	Multi-scan (*SADABS*; Sheldrick, 1996)
T_{min}, T_{max}	0.970, 0.977
No. of measured, independent and observed [$I > 2\sigma(I)$] reflections	13082, 3233, 2621
R_{int}	0.041
(sin $\theta/\lambda)_{max}$ (Å^{-1})	0.650
Refinement	
$R[F^2 > 2\sigma(F^2)]$, $wR(F^2)$, S	0.037, 0.093, 1.04
No. of reflections	3233
No. of parameters	200
No. of restraints	3
H-atom treatment	H atoms treated by a mixture of independent and constrained refinement
$\Delta\rho_{max}$, $\Delta\rho_{min}$ (e Å^{-3})	0.33, −0.25

Computer programs: *SMART* and *SAINT* (Bruker, 2008), *SHELXS97* (Sheldrick, 2015*a*), *SHELXL2014*/7 (Sheldrick, 2015*b*), *ORTEP-3 for Windows* (Farrugia, 2012), *DIAMOND* (Brandenburg, 2006) and *publCIF* (Westrip, 2010).

9. Refinement

Crystal data, data collection and structure refinement details are summarized in Table 7. Carbon-bound H atoms were placed in calculated positions (C—H = 0.95–0.99 Å) and were included in the refinement in the riding-model approximation, with U_{iso}(H) set to 1.2U_{eq}(C). The O- and N-bound H atoms were located from a difference map and refined with O—H and N—H = 0.84±0.01 and 0.88±0.01 Å, respectively, and with U_{iso}(H) = 1.5U_{eq}(O) and 1.2U_{eq}(N).

Funding information

Crystallographic research at Sunway University is supported by Sunway University Sdn Bhd (grant No. STR-RCTR-RCCM-001-2019).

References

Barolli, J. P., Maia, P. I. S., Colina-Vegas, L., Moreira, J., Plutin, A. M., Mocelo, R., Deflon, V. M., Cominetti, M. R., Camargo-Mathias, M. I. & Batista, A. A. (2017). *Polyhedron*, **126**, 33–41.
Bauzá, A., Ramis, R. & Frontera, A. (2014). *J. Phys. Chem. A*, **118**, 2827–2834.
Binzet, G., Gumus, I., Dogen, A., Flörke, U., Kulcu, N. & Arslan, H. (2018). *J. Mol. Struct.* **1161**, 519–529.
Brandenburg, K. (2006). *DIAMOND*. Crystal Impact GbR, Bonn, Germany.
Bruker (2008). *SMART* and *SAINT*. Bruker AXS Inc., Madison, Wisconsin, USA.
Chai, J. D. & Head-Gordon, M. (2008). *Phys. Chem. Chem. Phys.* **10**, 6615–6620.
Contreras-García, J., Johnson, E. R., Keinan, S., Chaudret, R., Piquemal, J. P., Beratan, D. N. & Yang, W. (2011). *J. Chem. Theory Comput.* **7**, 625–632.
Cornejo, J. A., Ayala, K., Richter, R., Böhlig, H., Hennig, L. & Beyer, L. (2005). *Z. Anorg. Allg. Chem.* **631**, 3040–3045.
Farrugia, L. J. (2012). *J. Appl. Cryst.* **45**, 849–854.
Frisch, M. J., *et al.* (2016). *GAUSSIAN16*. Revision A. 03. Gaussian, Inc., Wallingford CT, USA.
Gemili, M., Sari, H., Ulger, M., Sahin, E. & Nural, Y. (2017). *Inorg. Chim. Acta*, **463**, 88–96.
Gunasekaran, N., Jerome, P., Ng, S. W., Tiekink, E. R. T. & Karvembu, R. (2012). *J. Molec. Catal. A: Chem.* **353–354**, 156–162.
Gunasekaran, N., Ng, S. W., Tiekink, E. R. T. & Karvembu, R. (2012). *Polyhedron*, **34**, 41–45.
Gunasekaran, N., Vadivel, V., Halcovitch, N. R. & Tiekink, E. R. T. (2017). *Chem. Data Coll.* **9-10**, 263–276.
Hennig, L., Ayala-Leon, K., Angulo-Cornejo, J., Richter, R. & Beyer, L. (2009). *J. Fluor. Chem.* **130**, 453–460.
Huang, L., Massa, L. & Karle, J. (2008). *Proc. Natl Acad. Sci.* **105**, 13720–13723.
Jelsch, C., Ejsmont, K. & Huder, L. (2014). *IUCrJ*, **1**, 119–128.
Jeyalakshmi, K., Haribabu, J., Balachandran, C., Narmatha, E., Bhuvanesh, N. S. P., Aoki, S., Awale, S. & Karvembu, R. (2019). *New J. Chem.* **43**, 3188–3198.
Johnson, E. R., Keinan, S., Mori-Sánchez, P., Contreras-García, J., Cohen, A. J. & Yang, W. (2010). *J. Am. Chem. Soc.* **132**, 6498–6506.
Koch, K. R., Sacht, C. & Bourne, S. (1995). *Inorg. Chim. Acta*, **232**, 109–115.
Macrae, C. F., Edgington, P. R., McCabe, P., Pidcock, E., Shields, G. P., Taylor, R., Towler, M. & van de Streek, J. (2006). *J. Appl. Cryst.* **39**, 453–457.
Nishikawa, T. (2018). *Tetrahedron Lett.* **59**, 216–223.
Peng, B., Gao, Z., Li, X., Li, T., Chen, G., Zhou, M. & Zhang, J. (2016). *J. Biol. Inorg. Chem.* **21**, 903–916.
Petersson, G. A., Bennett, A., Tensfeldt, T. G., Al–Laham, M. A., Shirley, W. A. & Mantzaris, J. (1988). *J. Chem. Phys.* **89**, 2193–2218.
Plutín, A. M., Alvarez, A., Mocelo, R., Ramos, R., Castellano, E. E., da Silva, M. M., Colina-Vegas, L., Pavan, F. R. & Batista, A. A. (2016). *Inorg. Chem. Commun.* **63**, 74–80.
Saeed, A., Flörke, U. & Erben, M. F. (2014). *J. Sulfur Chem.* **35**, 318–355.
Saeed, A., Larik, F. A., Jabeen, F., Mehfooz, H., Ghumro, S. A., El-Seedi, H. R., Ali, M., Channar, P. A. & Ashraf, H. (2018). *Russ. J. Gen. Chem.* **88**, 541–550.
Selvakumaran, N., Karvembu, R., Ng, S. W. & Tiekink, E. R. T. (2011). *Acta Cryst.* E**67**, o602.
Selvakumaran, N., Ng, S. W., Tiekink, E. R. T. & Karvembu, R. (2011). *Inorg. Chim. Acta*, **376**, 278–284.
Sheldrick, G. M. (1996). *SADABS*. University of Göttingen, Germany.
Sheldrick, G. M. (2015*a*). *Acta Cryst.* A**71**, 3–8.
Sheldrick, G. M. (2015*b*). *Acta Cryst.* C**71**, 3–8.
Tan, S. L., Azizan, A. H. S., Jotani, M. M. & Tiekink, E. R. T. (2019). *Acta Cryst.* E**75**, 1472–1478.
Tan, S. L., Jotani, M. M. & Tiekink, E. R. T. (2019). *Acta Cryst.* E**75**, 308–318.
Turner, M. J., Mckinnon, J. J., Wolff, S. K., Grimwood, D. J., Spackman, P. R., Jayatilaka, D. & Spackman, M. A. (2017). *Crystal Explorer 17*. The University of Western Australia.
Westrip, S. P. (2010). *J. Appl. Cryst.* **43**, 920–925.
Woon, D. E. & Dunning, T. H. Jr (1993). *J. Chem. Phys.* **98**, 1358–1371.
Zhang, Z. & Schreiner, P. R. (2009). *Chem. Soc. Rev.* **38**, 1187–1198.

supporting information

Acta Cryst. (2020). E**76**, 155-161 [https://doi.org/10.1107/S2056989019017328]

3,3-Bis(2-hydroxyethyl)-1-(4-nitrobenzoyl)thiourea: crystal structure, Hirshfeld surface analysis and computational study

Sang Loon Tan, Mukesh M. Jotani and Edward R. T. Tiekink

Computing details

Data collection: *SMART* (Bruker, 2008); cell refinement: *SAINT* (Bruker, 2008); data reduction: *SAINT* (Bruker, 2008); program(s) used to solve structure: *SHELXS97* (Sheldrick, 2015*a*); program(s) used to refine structure: *SHELXL2014*/7 (Sheldrick, 2015*b*); molecular graphics: *ORTEP-3 for Windows* (Farrugia, 2012), *DIAMOND* (Brandenburg, 2006); software used to prepare material for publication: *publCIF* (Westrip, 2010).

(I)

Crystal data

$C_{12}H_{15}N_3O_5S$
$M_r = 313.33$
Monoclinic, $P2_1/c$
$a = 7.4203$ (2) Å
$b = 10.3241$ (3) Å
$c = 18.4191$ (6) Å
$\beta = 95.471$ (2)°
$V = 1404.62$ (7) Å^3
$Z = 4$
$F(000) = 656$
$D_x = 1.482$ Mg m^{-3}
Mo $K\alpha$ radiation, $\lambda = 0.71073$ Å
Cell parameters from 2434 reflections
$\theta = 2.3$–25.8°
$\mu = 0.26$ mm^{-1}
$T = 100$ K
Block, pale yellow
0.12 × 0.11 × 0.09 mm

Data collection

Bruker SMART APEX diffractometer
Radiation source: fine-focus sealed tube
Graphite monochromator
φ and ω scans
Absorption correction: multi-scan (SADABS; Sheldrick, 1996)
$T_{min} = 0.970$, $T_{max} = 0.977$
13082 measured reflections
3233 independent reflections
2621 reflections with $I > 2\sigma(I)$
$R_{int} = 0.041$
$\theta_{max} = 27.5°$, $\theta_{min} = 2.2°$
$h = -9\rightarrow9$
$k = -13\rightarrow13$
$l = -23\rightarrow23$

Refinement

Refinement on F^2
Least-squares matrix: full
$R[F^2 > 2\sigma(F^2)] = 0.037$
$wR(F^2) = 0.093$
$S = 1.04$
3233 reflections
200 parameters
3 restraints
Primary atom site location: structure-invariant direct methods
Secondary atom site location: difference Fourier map
Hydrogen site location: mixed
H atoms treated by a mixture of independent and constrained refinement
$w = 1/[\sigma^2(F_o^2) + (0.042P)^2 + 0.3083P]$ where $P = (F_o^2 + 2F_c^2)/3$
$(\Delta/\sigma)_{max} = 0.001$
$\Delta\rho_{max} = 0.33$ e Å^{-3}
$\Delta\rho_{min} = -0.25$ e Å^{-3}

Special details

Geometry. All esds (except the esd in the dihedral angle between two l.s. planes) are estimated using the full covariance matrix. The cell esds are taken into account individually in the estimation of esds in distances, angles and torsion angles; correlations between esds in cell parameters are only used when they are defined by crystal symmetry. An approximate (isotropic) treatment of cell esds is used for estimating esds involving l.s. planes.

Fractional atomic coordinates and isotropic or equivalent isotropic displacement parameters (Å²)

	x	*y*	*z*	U_{iso}*/U_{eq}
S1	0.74915 (5)	0.45567 (4)	0.59498 (2)	0.02217 (12)
O1	0.72148 (15)	0.75229 (11)	0.77993 (8)	0.0313 (3)
H1O	0.760 (3)	0.8221 (13)	0.7992 (11)	0.047*
O2	0.16441 (15)	0.47542 (11)	0.65347 (6)	0.0219 (3)
H2O	0.0554 (16)	0.466 (2)	0.6367 (12)	0.051 (7)*
O3	0.88241 (15)	0.29890 (10)	0.73714 (6)	0.0221 (3)
O4	1.35804 (19)	0.56698 (14)	1.06330 (7)	0.0407 (4)
O5	1.3728 (2)	0.35951 (15)	1.07036 (8)	0.0538 (4)
N1	0.52846 (17)	0.57554 (12)	0.67890 (7)	0.0168 (3)
N2	0.80071 (17)	0.51231 (12)	0.73839 (7)	0.0174 (3)
H2N	0.801 (2)	0.5824 (12)	0.7648 (8)	0.021*
N3	1.3235 (2)	0.45902 (16)	1.03874 (8)	0.0300 (4)
C1	0.6860 (2)	0.51602 (14)	0.67325 (8)	0.0167 (3)
C2	0.4669 (2)	0.61682 (14)	0.74939 (8)	0.0181 (3)
H2A	0.5141	0.5555	0.7879	0.022*
H2B	0.3330	0.6135	0.7461	0.022*
C3	0.5291 (2)	0.75230 (15)	0.77061 (10)	0.0232 (4)
H3A	0.4853	0.8146	0.7320	0.028*
H3B	0.4800	0.7783	0.8166	0.028*
C4	0.4055 (2)	0.60787 (16)	0.61391 (8)	0.0211 (3)
H4A	0.4779	0.6236	0.5723	0.025*
H4B	0.3402	0.6889	0.6232	0.025*
C5	0.2690 (2)	0.50167 (17)	0.59362 (9)	0.0224 (3)
H5A	0.1876	0.5288	0.5506	0.027*
H5B	0.3329	0.4220	0.5807	0.027*
C6	0.89516 (19)	0.40521 (14)	0.76552 (8)	0.0163 (3)
C7	1.0107 (2)	0.42635 (14)	0.83615 (8)	0.0172 (3)
C8	1.0674 (2)	0.54755 (15)	0.86196 (9)	0.0205 (3)
H8	1.0348	0.6228	0.8340	0.025*
C9	1.1712 (2)	0.55922 (16)	0.92821 (9)	0.0229 (4)
H9	1.2105	0.6417	0.9463	0.027*
C10	1.2160 (2)	0.44763 (17)	0.96720 (9)	0.0225 (4)
C11	1.1652 (2)	0.32570 (16)	0.94236 (9)	0.0249 (4)
H11	1.2000	0.2507	0.9702	0.030*
C12	1.0628 (2)	0.31546 (15)	0.87614 (9)	0.0222 (3)
H12	1.0275	0.2325	0.8576	0.027*

Atomic displacement parameters (Å²)

	U^{11}	U^{22}	U^{33}	U^{12}	U^{13}	U^{23}
S1	0.0180 (2)	0.0320 (2)	0.0167 (2)	0.00001 (16)	0.00252 (15)	−0.00347 (16)
O1	0.0161 (6)	0.0216 (6)	0.0562 (9)	−0.0018 (5)	0.0031 (6)	−0.0148 (6)
O2	0.0150 (6)	0.0302 (6)	0.0202 (6)	−0.0025 (5)	0.0007 (5)	0.0039 (5)
O3	0.0206 (6)	0.0177 (6)	0.0274 (6)	0.0012 (4)	−0.0010 (5)	−0.0045 (5)
O4	0.0425 (8)	0.0469 (8)	0.0303 (7)	−0.0041 (7)	−0.0090 (6)	−0.0105 (6)
O5	0.0680 (11)	0.0522 (9)	0.0356 (8)	−0.0006 (8)	−0.0231 (8)	0.0156 (7)
N1	0.0158 (6)	0.0181 (6)	0.0166 (6)	0.0005 (5)	0.0015 (5)	0.0018 (5)
N2	0.0171 (7)	0.0172 (6)	0.0177 (6)	0.0020 (5)	0.0000 (5)	−0.0032 (5)
N3	0.0241 (8)	0.0442 (10)	0.0212 (7)	−0.0019 (7)	−0.0010 (6)	0.0024 (7)
C1	0.0150 (7)	0.0157 (7)	0.0190 (8)	−0.0025 (6)	0.0003 (6)	0.0011 (6)
C2	0.0167 (8)	0.0183 (7)	0.0198 (7)	0.0008 (6)	0.0035 (6)	−0.0007 (6)
C3	0.0162 (8)	0.0208 (8)	0.0324 (9)	0.0023 (6)	0.0009 (7)	−0.0043 (7)
C4	0.0178 (8)	0.0258 (8)	0.0191 (8)	0.0014 (6)	−0.0007 (6)	0.0069 (7)
C5	0.0169 (8)	0.0334 (9)	0.0167 (8)	−0.0003 (7)	0.0010 (6)	0.0013 (7)
C6	0.0125 (7)	0.0175 (7)	0.0193 (7)	−0.0003 (6)	0.0041 (6)	−0.0001 (6)
C7	0.0136 (7)	0.0198 (8)	0.0187 (8)	0.0012 (6)	0.0038 (6)	0.0008 (6)
C8	0.0188 (8)	0.0194 (8)	0.0228 (8)	−0.0006 (6)	0.0003 (6)	0.0034 (6)
C9	0.0215 (8)	0.0223 (8)	0.0243 (8)	−0.0039 (6)	−0.0001 (7)	−0.0029 (7)
C10	0.0174 (8)	0.0329 (9)	0.0169 (8)	0.0008 (7)	−0.0005 (6)	0.0005 (7)
C11	0.0257 (9)	0.0238 (8)	0.0248 (8)	0.0049 (7)	0.0004 (7)	0.0077 (7)
C12	0.0224 (8)	0.0185 (8)	0.0254 (8)	0.0027 (6)	0.0008 (7)	−0.0001 (6)

Geometric parameters (Å, º)

S1—C1	1.6777 (16)	C3—H3A	0.9900
O1—C3	1.4218 (19)	C3—H3B	0.9900
O1—H1O	0.843 (10)	C4—C5	1.515 (2)
O2—C5	1.4331 (19)	C4—H4A	0.9900
O2—H2O	0.844 (10)	C4—H4B	0.9900
O3—C6	1.2156 (18)	C5—H5A	0.9900
O4—N3	1.221 (2)	C5—H5B	0.9900
O5—N3	1.220 (2)	C6—C7	1.504 (2)
N1—C1	1.334 (2)	C7—C8	1.389 (2)
N1—C4	1.4723 (19)	C7—C12	1.396 (2)
N1—C2	1.4796 (19)	C8—C9	1.385 (2)
N2—C6	1.3771 (19)	C8—H8	0.9500
N2—C1	1.4038 (19)	C9—C10	1.381 (2)
N2—H2N	0.871 (9)	C9—H9	0.9500
N3—C10	1.479 (2)	C10—C11	1.379 (2)
C2—C3	1.512 (2)	C11—C12	1.378 (2)
C2—H2A	0.9900	C11—H11	0.9500
C2—H2B	0.9900	C12—H12	0.9500
C3—O1—H1O	110.5 (15)	C5—C4—H4B	109.1
C5—O2—H2O	108.2 (16)	H4A—C4—H4B	107.8

C1—N1—C4	121.38 (13)	O2—C5—C4	110.21 (13)
C1—N1—C2	123.19 (13)	O2—C5—H5A	109.6
C4—N1—C2	115.41 (12)	C4—C5—H5A	109.6
C6—N2—C1	125.31 (13)	O2—C5—H5B	109.6
C6—N2—H2N	119.3 (11)	C4—C5—H5B	109.6
C1—N2—H2N	115.1 (11)	H5A—C5—H5B	108.1
O5—N3—O4	123.33 (16)	O3—C6—N2	123.57 (14)
O5—N3—C10	118.05 (15)	O3—C6—C7	121.17 (13)
O4—N3—C10	118.63 (15)	N2—C6—C7	115.20 (13)
N1—C1—N2	114.23 (13)	C8—C7—C12	119.91 (14)
N1—C1—S1	123.83 (12)	C8—C7—C6	123.75 (14)
N2—C1—S1	121.89 (11)	C12—C7—C6	116.34 (14)
N1—C2—C3	112.40 (13)	C9—C8—C7	120.31 (15)
N1—C2—H2A	109.1	C9—C8—H8	119.8
C3—C2—H2A	109.1	C7—C8—H8	119.8
N1—C2—H2B	109.1	C10—C9—C8	118.14 (15)
C3—C2—H2B	109.1	C10—C9—H9	120.9
H2A—C2—H2B	107.9	C8—C9—H9	120.9
O1—C3—C2	108.01 (12)	C11—C10—C9	122.97 (15)
O1—C3—H3A	110.1	C11—C10—N3	118.37 (15)
C2—C3—H3A	110.1	C9—C10—N3	118.66 (15)
O1—C3—H3B	110.1	C12—C11—C10	118.26 (15)
C2—C3—H3B	110.1	C12—C11—H11	120.9
H3A—C3—H3B	108.4	C10—C11—H11	120.9
N1—C4—C5	112.61 (13)	C11—C12—C7	120.37 (15)
N1—C4—H4A	109.1	C11—C12—H12	119.8
C5—C4—H4A	109.1	C7—C12—H12	119.8
N1—C4—H4B	109.1		

C4—N1—C1—N2	169.47 (13)	O3—C6—C7—C12	−16.0 (2)
C2—N1—C1—N2	−8.8 (2)	N2—C6—C7—C12	161.02 (14)
C4—N1—C1—S1	−8.0 (2)	C12—C7—C8—C9	−1.8 (2)
C2—N1—C1—S1	173.80 (11)	C6—C7—C8—C9	178.89 (14)
C6—N2—C1—N1	134.76 (15)	C7—C8—C9—C10	0.1 (2)
C6—N2—C1—S1	−47.8 (2)	C8—C9—C10—C11	1.4 (3)
C1—N1—C2—C3	89.24 (17)	C8—C9—C10—N3	−178.75 (15)
C4—N1—C2—C3	−89.11 (16)	O5—N3—C10—C11	4.8 (2)
N1—C2—C3—O1	−62.76 (17)	O4—N3—C10—C11	−174.96 (16)
C1—N1—C4—C5	91.30 (17)	O5—N3—C10—C9	−175.05 (17)
C2—N1—C4—C5	−90.33 (16)	O4—N3—C10—C9	5.2 (2)
N1—C4—C5—O2	57.76 (17)	C9—C10—C11—C12	−1.1 (3)
C1—N2—C6—O3	−3.6 (2)	N3—C10—C11—C12	179.10 (15)
C1—N2—C6—C7	179.39 (13)	C10—C11—C12—C7	−0.8 (2)
O3—C6—C7—C8	163.29 (15)	C8—C7—C12—C11	2.2 (2)
N2—C6—C7—C8	−19.7 (2)	C6—C7—C12—C11	−178.47 (14)

Hydrogen-bond geometry (Å, º)

*Cg*1 is the centroid of the (C7–C12) ring.

D—H···*A*	*D*—H	H···*A*	*D*···*A*	*D*—H···*A*
N2—H2*N*···O1	0.87 (1)	1.88 (1)	2.6749 (17)	151 (1)
O1—H1*O*···O2^{i}	0.84 (2)	1.87 (2)	2.7075 (17)	176 (2)
O2—H2*O*···S1^{ii}	0.84 (1)	2.33 (1)	3.1724 (12)	175 (2)
C2—H2*B*···O3^{i}	0.99	2.53	3.2305 (18)	127
C5—H5*A*···S1^{iii}	0.99	2.77	3.4915 (17)	130
C8—H8···O3^{iv}	0.95	2.36	3.2147 (19)	150
N3—O4···*Cg*1^{v}	1.22 (1)	3.63 (1)	3.6927 (16)	83 (1)

Symmetry codes: (i) −*x*+1, *y*+1/2, −*z*+3/2; (ii) *x*−1, *y*, *z*; (iii) −*x*+1, −*y*+1, −*z*+1; (iv) −*x*+2, *y*+1/2, −*z*+3/2; (v) −*x*+2, −*y*+1, −*z*+2.